

# COMPUTATION OF MASS-OUTFLOW RATES FROM ADVECTIVE ACCRETION DISKS AROUND BLACK HOLES

TAPAS K. DAS

*S. N. Bose National Centre For Basic Sciences  
JD Block, Salt Lake, Sector-III, Calcutta-700091,  
India  
e-mail:tdas@boson.bose.res.in*

Appearing in ‘Observational Evidence for Black Holes in the Universe’, Ed. S.K. Chakrabarti (Kluwer Academic Publishers: Holland), p. 113, (1998).

## 1. Introduction

The existing models which study the origin, acceleration and collimation of mass outflow in the form of jets from AGNs and Quasars are roughly of three types. The first type of solutions confine themselves to the jet properties only, completely decoupled from the internal properties of accretion disks (see, e.g., Begelman, Blandford & Rees, 1984). In the second type, efforts are made to correlate the internal disk structure with that of the outflow using both hydrodynamic (e.g., Chakrabarti 1986) and magnetohydrodynamic considerations (Königl 1989; Chakrabarti & Bhaskaran 1992). In the third type, numerical simulations are carried out to actually see how matter is deflected from the equatorial plane towards the axis (e.g., Hawley, Smarr & Wilson, 1984, 1985; Eggum, Katz & Coroniti, 1985; Molteni, Lanzafame & Chakrabarti, 1994, hereafter MLC94; Molteni, Ryu & Chakrabarti, 1996, hereafter MRC96; Ryu, Chakrabarti & Molteni, 1997; Nobuta & Hanawa, 1998). From the analytical front, although the wind type solutions and accretion type solutions come out of the same set of governing equations (Chakrabarti 1990), there are few, and mostly qualitative attempt to find connections among them (Chakrabarti, 1997a). As a result, the estimation of the outflow rate from the inflow rate has been difficult. Our work, *for the first time*, quantitatively connects the topologies of the inflow and the outflow. The simplicity of black holes and neutron stars lie in the fact that they do not have atmospheres. But the disks surrounding them have, and similar method as employed in stellar atmospheres should

be applicable to the disks. Our approach in this paper is precisely this. We first determine the properties of the rotating inflow and outflow and identify solutions to connect them. In this manner, we self-consistently determine the mass outflow rates.

Before we present our results, we describe basic properties of the rotating inflow and outflow. As is well known (MLC94, MRC96 and references therein), in the centrifugal pressure supported boundary layer (CENBOL) the flow becomes hotter and denser and for all practical purposes behaves as the stellar atmosphere so far as the formation of outflows are concerned. In case where the shock does not form, regions around pressure maximum achieved just outside the inner sonic point would also drive the flow outwards. We calculate the mass outflow rates ( $R_{\dot{m}}$ ) rate as a function of the inflow parameters, such as specific energy and angular momentum, accretion rate, polytropic index etc. We explore both the polytropic and the isothermal outflows. A detailed report on this type of outflows is presented elsewhere (Das & Chakrabarti, 1998, hereafter DC98).

The plan of this paper is the following: In the next Section, we describe our model and present the governing equations for the inflow and outflow. We also provide the solution procedure of those equations. In §3, we present results of our computations. Finally, in §4, we draw our conclusions.

## 2. Model Description, Governing Equations and the solution Procedure

We consider thin, axisymmetric polytropic inflows in vertical equilibrium (otherwise known as 1.5 dimensional flow). We ignore the self-gravity of the flow and viscosity is assumed to be significant only at the shock so that entropy is generated. We do the calculations using Paczyński-Wiita (1980) potential which mimics surroundings of the Schwarzschild black hole. The equations (in dimensionless units) governing the inflow are:

$$\mathcal{E} = \frac{u_e^2}{2} + n a_e^2 + \frac{\lambda^2}{2r^2} - \frac{1}{2(r-1)}. \quad (1)$$

$$\dot{M}_{in} = u_e \rho_e r h_e(r), \quad (2)$$

(For detail, see, Chakrabarti, 1989 hereafter C89). The equations governing the polytropic outflow are

$$\mathcal{E} = \frac{\vartheta^2}{2} + n' a_e^2 + \frac{\lambda^2}{2r_m^2(r)} - \frac{1}{2(r-1)} \quad (3)$$

And

$$\dot{M}_{out} = \rho \vartheta \mathcal{A}(r). \quad (4)$$

Where  $r_m$  is the mean axial distance of the flow and  $\mathcal{A}(r)$  is the cross sectional area through which mass is flowing out. (For detail, see, DC98.)  $\gamma$  of the outflow was taken to be smaller than that of the inflow because of momentum deposition effects. The outflow angular momentum  $\lambda$  is chosen to be the same as in the inflow, i.e., no viscous dissipation is assumed to be present in the inner region of the flow close to a black hole. Considering that viscous time scales are longer compared to the inflow time scale, it may be a good assumption in the disk, but it may not be a very good assumption for the outflows which are slow prior to the acceleration and are therefore, prone to viscous transport of angular momentum. Detailed study of the outflow rates in presence of viscosity and magnetic field is in progress and would be presented elsewhere. The Isothermal outflow is governed by the following equations

$$\frac{\vartheta_{iso}^2}{2} + C_s^2 \ln \rho + \frac{\lambda^2}{2r_m(r)^2} - \frac{1}{2(r-1)} = \text{Constant} \quad (5)$$

And

$$\dot{M}_{out} = \rho \vartheta_{iso} \mathcal{A}(r). \quad (6)$$

Here, the area function remains the same above. A subscript *iso* of velocity  $\vartheta$  is kept to distinguish from the velocity in the polytropic case. This is to indicate the velocities are measured here using completely different assumptions. For details, see DC98.

In both the models of the outflow, we assume that the flow is primarily radial. Thus the  $\theta$ -component of the velocity is ignored ( $\vartheta_\theta \ll \vartheta$ ).

## 2.1. PROCEDURE TO SOLVE FOR DISKS AND OUTFLOWS SIMULTANEOUSLY

For polytropic outflows, we solve equations (1-4) simultaneously using numerical techniques (for detail, see, DC98). In this case the specific energy  $\mathcal{E}$  is assumed to remain fixed throughout the flow trajectory as it moves from the disk to the jet. At the shock, entropy is generated and hence the outflow is of higher entropy for the same specific energy.

A supply of parameters  $\mathcal{E}$ ,  $\lambda$ ,  $\gamma$  and  $\gamma_o$  makes a self-consistent computation of  $R_m$  possible when the shock is present. In the case where the shocks do not form, the procedure is a bit different. It is assumed that the maximum amount of matter comes out from the place of the disk where the thermal pressure of the inflow attains its maximum and the outflow is assumed to have the same quasi-conical shape with annular cross-section  $\mathcal{A}(r)$  between the funnel wall and the centrifugal barrier as already defined. For this case, the compression ratio of the gas at the pressure maximum between the inflow and outflow  $R_{comp}$  is supplied as a free parameter, since

it may be otherwise very difficult to compute satisfactorily. In the presence of shocks, such problems do not arise as the compression ratio is obtained self-consistently. For isothermal outflow, it is assumed that the outflow has exactly the *same* temperature as that of the post-shock flow, but the energy is not conserved as matter goes from disk to the wind. The polytropic index of the inflow can vary but that of the outflow is always unity. The other assumptions and logical steps are exactly same as those of the case where the outflow is polytropic. Here we solve equations (1-2) and (5-6) simultaneously using numerical technique to get results. (For details, see, DC98).

### 3. Results

#### 3.1. POLYTROPIC OUTFLOW COMING FROM THE POST-SHOCK ACCRETION DISK

Figure 1 shows a typical solution which combines the accretion and the outflow. The input parameters are  $\mathcal{E} = 0.00689$ ,  $\lambda = 1.65$  and  $\gamma = 4/3$  corresponding to relativistic inflow (see Fig. 5 and 6 of C89). The solid curve with an arrow represents the pre-shock region of the inflow and the long-dashed curve represents the post-shock inflow which enters the black hole after passing through the inner sonic point (I). The solid vertical line at  $X_{s3}$  with double arrow represents the shock transition. Three dotted curves represent three outflow solutions for the parameters  $\gamma_o = 1.3$  (top), 1.1 (middle) and 1.03 (bottom). The outflow branches shown pass through the corresponding sonic points. It is evident from the figure that the outflow moves along solution curves which are completely different from that of the ‘wind solution’ of the inflow which passes through the outer sonic point ‘O’. The mass loss ratio  $R_{\dot{m}}$  in these cases are 0.47, 0.22 and 0.06 respectively. Figure 2 shows the ratio  $R_{\dot{m}}$  as  $\gamma_o$  is varied. Only the range of  $\gamma_o$  for which the shock-solution is present is shown here. In Fig. 3a we show the variation of the ratio  $R_{\dot{m}}$  of the mass outflow rate inflow rate as a function of the shock-strength (solid)  $M_-/M_+$  (Here,  $M_-$  and  $M_+$  are the Mach numbers of the pre- and post-shock flows respectively.), the compression ratio (dotted)  $\Sigma_+/\Sigma_-$  (Here,  $\Sigma_-$  and  $\Sigma_+$  are the vertically integrated matter densities in the pre- and post- shock flows respectively), and the stable shock location (dashed)  $X_{s3}$  (in the notation of C89). Other parameters are  $\lambda = 1.75$  and  $\gamma_o = 1.1$ . Note that the ratio  $R_{\dot{m}}$  does not peak near the strongest shocks! Shocks are stronger when they are located closer to the black hole, i.e., for smaller energies. In Fig. 3b where  $R_{\dot{m}}$  is plotted as a function of the specific energy  $\mathcal{E}$  (along x-axis) and  $\gamma_o$  (marked on each curve). Specific angular momentum is chosen to be  $\lambda = 1.75$  as before. The peak in  $R_{\dot{m}}$  is observed (see also, Chakrabarti, 1997a, and Chakrabarti, this volume).

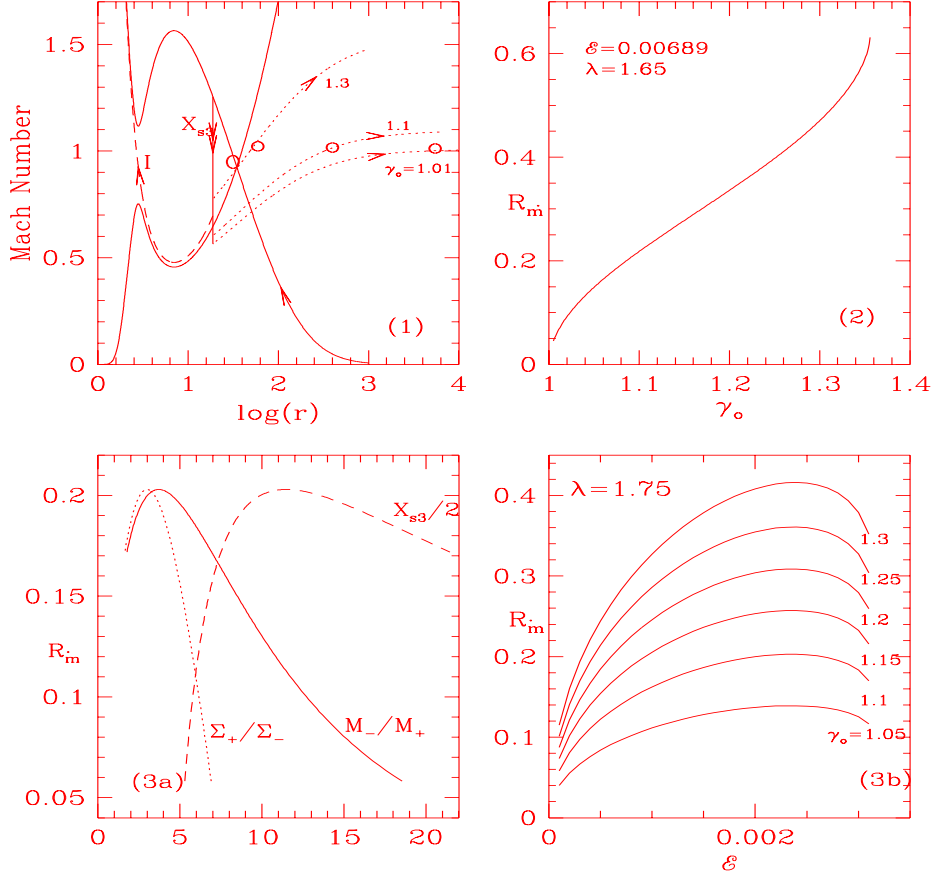


**Fig. 1-3:** Mach number of the flow is plotted against logarithmic radial distance both for the inflow and outflow (Fig. 1). The ratio of mass outflow rate and mass inflow rate is plotted against the polytropic index of the outflow (Fig. 2). The same ratio is plotted against the shock strength, shock location and the ratio of the integrated density (Fig. 3a) and specific energy  $\epsilon$  and polytropic index of the outgoing flow  $\gamma_o$  (Fig. 3b). See text for details.

To have a better insight of the behavior of the outflow we plot in Fig. 4  $R_m$  as a function of the polytropic index of the incoming flow  $\gamma$ . The range of  $\gamma$  shown is the range for which shock forms in the flow. We also plot the variation of velocity  $v_o$ , density  $\rho_o$  and area  $A(r)$  of the outflow at the location where the outflow leaves the disk. These quantities are scaled from

the corresponding dimensionless units as  $\vartheta_o \rightarrow 2 \times 10^4 \vartheta_o - 558$ ,  $\rho_o \rightarrow 10^{22} \rho_o$  and  $\mathcal{A} \rightarrow 0.0005 \mathcal{A}$  respectively in order to bring them in the same scale. The non-monotonic nature of the variation of  $R_{\dot{m}}$  with  $\gamma$  is observed.

### 3.2. POLYTROPIC OUTFLOW COMING FROM THE REGION OF THE MAXIMUM PRESSURE

In this case, the inflow parameters are chosen from region **I** (see C89) so that the shocks do not form. Here, the inflow passes through the inner sonic point only. The outflow is assumed to be coming out from the regions where the polytropic inflow has maximum pressure. Figure 5a shows a typical solution. The arrowed solid curve shows the inflow and the dotted arrowed curves show the outflows for  $\gamma_o = 1.3$  (top), 1.1 (middle) and 1.01 (bottom). The ratio  $R_{\dot{m}}$  in these cases is given by 0.66, 0.30 and 0.09 respectively. The specific energy and angular momentum are chosen to be  $\mathcal{E} = 0.00584$  and  $\lambda = 1.8145$  respectively. The pressure maximum occurs outside the inner sonic point at  $r_m$  when the flow is still subsonic. Figure 5b shows the variation of thermal pressure of the flow with radial distance. The peak is clearly visible. Figure 6 shows the ratio  $R_{\dot{m}}$  as a function of  $\gamma_o$  for various choices of the compression ratio  $R_{comp}$  of the outflowing gas at the pressure maximum:  $R_{comp} = 2$  for the bottom curve and 7 for the top curve. Note that flows with highest compression ratios produce highest outflow rates, evacuating the disk which is responsible for the quiescent states in X-ray Novae systems and also in some systems with massive black holes (e.g., our own galactic centre?).

The location of maximum pressure being close to the black hole, it may be very difficult to generate the outflow from this region. Thus, it is expected that the ratio  $R_{\dot{m}}$  would be larger when the maximum pressure is located farther out. This is exactly what we see in Fig. 7, where we plot  $R_{\dot{m}}$  against the location of the pressure maximum (solid curve). Secondly, if our guess that the outflow rate could be related to the pressure is correct, then the rate should increase as the pressure at the maximum rises. That's also what we observe in Fig. 7. We plot  $R_{\dot{m}}$  as a function of the actual pressure at the pressure maximum (dotted curve). The mass loss is found to be a strongly correlated with the thermal pressure. Here we have multiplied non-dimensional thermal pressure by  $1.5 \times 10^{24}$  in order to bring them in the same scale.

### 3.3. ISOTHERMAL OUTFLOW COMING FROM THE POST-SHOCK ACCRETION DISK

Here the temperature of the outflow is obtained from the proton temperature of the advective region of the disk. The proton temperature is ob-

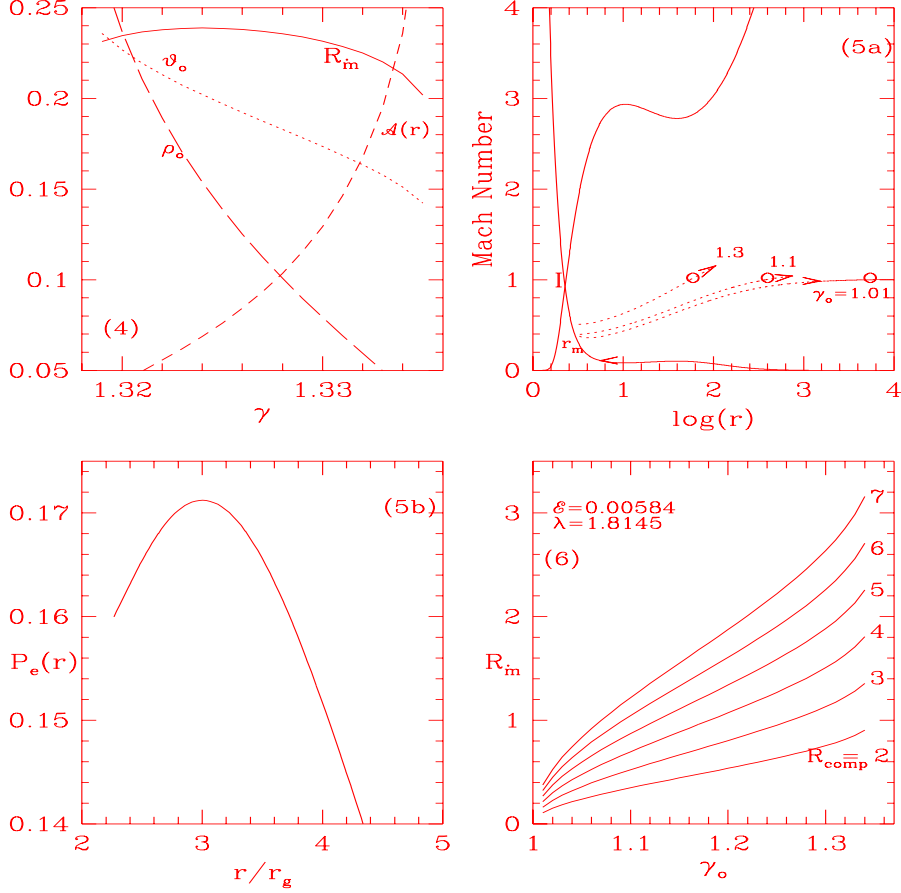


**Fig. 4-6:** Variation of velocity, density, cross sectional area and the rate ratio as a function of the polytropic index of the inflow (Fig. 4). Variation of the Mach number for inflow and outflow when shocks are not present (Fig. 5a). Thermal pressure variation as a function of the radial distance  $r/r_g$  showing a distinct maximum (Fig. 5b). Variation of  $R_{\dot{m}}$  when both the compression ratio at the pressure maxima and polytropic index of the outflow are changed (Fig. 6). See text for details.

tained using the Comptonization, bremsstrahlung, inverse bremsstrahlung and Coulomb processes (Chakrabarti, 1997b and references therein). Figure 8 shows the effective proton temperature and the electron temperature of the post-shock advective region as a function of the accretion rate (in

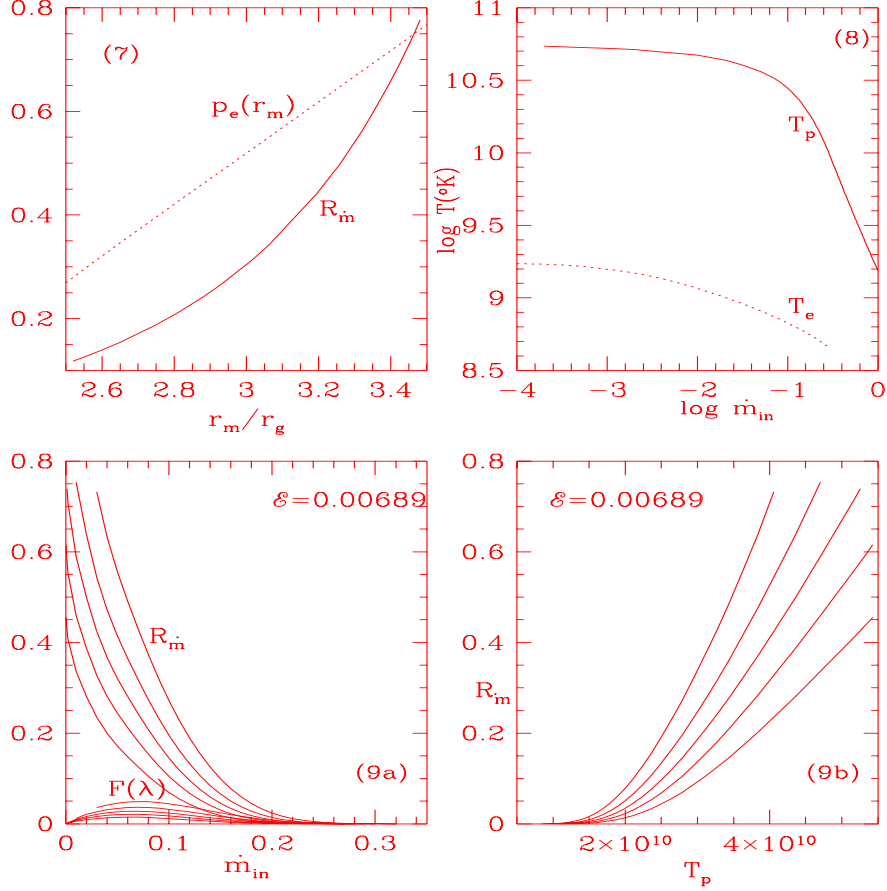


**Fig. 7-9:** Variation of the maximum pressure and  $R_m$  with the location where the pressure maxima occur (Fig. 7). Proton and electron temperatures in the advective region as a function of the inflow disk accretion rate  $\dot{m}_{in}$  (Fig. 8). Variation of the  $R_m$  and angular momentum flux  $F(\lambda)$  as a function of the accretion rate of the inflow (Fig. 9a). Variation of  $R_m$  with proton temperature  $T_p$  (Fig. 9b). See text for details.

logarithmic scale) of the Keplerian component of the disk. In Fig. 9a, we show the ratio  $R_m$  as a function of the Eddington rate of the incoming flow for a range of the specific angular momentum. In the low luminosity objects the ratio is larger. Angular momentum is varied from  $\lambda = 1.63$  (top curve) to 1.65 (bottom curve). An interval of  $\lambda = 0.005$  was used. The ratio is

very sensitive to the angular momentum since it changes the shock location rapidly and therefore changes the post-shock temperature very much. We also plot the outflux of angular momentum  $F(\lambda) = \lambda \dot{m}_{in} R_{in}$  which has a maximum at intermediate accretion rates. In dimensional units, these quantities represent significant fractions of angular momentum of the entire disk and therefore the rotating outflow can help accretion processes. Curves are drawn for different  $\lambda$  as above. In Fig. 9b, we plot the variation of the ratio directly with the proton temperature of the advecting region. The outflow is clearly thermally driven. Hotter flow produces more winds as is expected. The angular momentum associated with each curve is same as before.

### 3.4. ISOTHERMAL OUTFLOW COMING FROM THE REGION OF THE MAXIMUM PRESSURE

This case produces very similar result as in the above case, except that like Section 3.2 the outflow rate becomes more than a hundred percent of the inflow rate when the proton temperature is very high. This phenomenon may be responsible for producing quiescent states in some black hole candidates.

## 4. Conclusions

The basic conclusions of this paper are the followings:

- a) It is possible that most of the outflows are coming from the centrifugally supported boundary layer (CENBOL) of the accretion disks.
- b) The outflow rate generally increases with the proton temperature of CENBOL. In other words, winds are, at least partially, thermally driven. This is reflected more strongly when the outflow is isothermal.
- c) Even though specific angular momentum of the flow increases the size of the CENBOL, and one would have expected a higher mass flux in the wind, we find that the rate of the outflow is actually anti-correlated with the  $\lambda$  of the inflow. This is because the average proton temperature of CENBOL goes down with  $\lambda$ .
- (d) Presence of significant viscosity in CENBOL may reduce angular momentum of the outflow. When this is taken into account, we find that the rate of the outflow is correlated with  $\lambda$  of the outflow. This suggests that the outflow is partially centrifugally driven as well.
- e) The ratio  $R_{in}$  is generally anti-correlated with the inflow accretion rate. That is, disks of lower luminosity would produce higher ratio  $R_{in}$ .
- f) Generally speaking, supersonic region of the inflow do not have pressure maxima. Thus, outflows emerge from the subsonic region of the inflow,

whether the shock actually forms or not.

An interesting situation arises when the polytropic index of the outflow is large and the compression ratio of the flow is also very high. In this case, the flow virtually bounces back as the winds and the outflow rate can be temporarily larger compared with the inflow rate, thereby evacuating the disk. In this range of parameters, most, if not all, of our assumptions breakdown completely because the situation becomes inherently time-dependent. It is possible that some of the black hole systems, including that in our own galactic centre, may have undergone such evacuation phase in the past and gone into quiescent phase.

So far, we made the computations around a Schwarzschild black hole. The mass outflow rates for Kerr black holes are being studied and the results would be reported elsewhere (Das, 1998a). For the quasi-spherical Bondi-type accretion onto black holes, the accretion disk does not form, the freely falling matter may produce a standing collisionless shock due to the plasma instabilities and the nonlinearity introduced in the flow due to even a small density perturbation. Outflow from these cases is also being studied and would be reported elsewhere (Das, 1998b).

We made a few assumptions, some of which may be questionable. Nevertheless, we believe that our calculation is sufficiently illustrative and gives a direction which can be followed in the future.

## References

- Begelman, M.C., Blandford, R.D. & Rees, M.J. 1984, Rev. Mod. Phys., 56, 255  
 Chakrabarti, S. K. 1986, *Astrophys. J.*, 303, 582  
 Chakrabarti, S. K. 1989, *Astrophys. J.*, 347, 365  
 Chakrabarti, S. K. 1990, *Theory of Transonic Astrophysical Flows* (Singapore: World Sci.) (C90)  
 Chakrabarti, S.K., 1997a, *Astrophys. J.*, submitted  
 Chakrabarti, S. K. 1997b, *Astrophys. J.*, 484, 313  
 Chakrabarti, S. K. & Bhaskaran, P. 1992, *MNRAS*, 255, 255  
 Das, T.K. & Chakrabarti, S.K. 1998, *Astrophys. J.* (submitted)  
 Das, T.K. 1998a, in preparation  
 Das, T.K. 1998b, in preparation  
 Königl, A. 1989, *Astrophys. J.*, 342, 208  
 Hawley, J.W., Smarr, L. & Wilson, J. 1984, *Astrophys. J.*, 297, 296.  
 Hawley, J.F., Smarr, L.L., & Wilson, J.R. 1985, *Astrophys. J.*, 55, 211  
 Eggum, G. E., Coroniti, F. V., Katz, J. I. 1985, *Astrophys. J.*, 298, L41  
 Molteni, D., Lanzafame, G. & Chakrabarti, S. K. 1994 *Astrophys. J.*, 425, 161  
 Molteni, D., Ryu, D. & Chakrabarti, S.K. 1996 *Astrophys. J.* **470** 460  
 Paczyński, B. & Wiita, P.J. 1980 *Astron. Astrophys.*, **88**, 23  
 Ryu, D., Chakrabarti, S. K., & Molteni, D. 1997, *Astrophys. J.*, 474, 378